THE ASTROPHYSICAL JOURNAL, 461:742–749, 1996 April 20

SPATIAL DISTRIBUTIONS OF YOUNG LARGE MAGELLANIC CLOUD CLUSTERS AS TRACERS OF A BAR PERTURBATION

H. DOTTORI[1] AND E. BICA[1,2]
Instituto de Física, Universidade Federal do Rio Grande do Sul, Avenida Bento Gonçalves 9500, CEP 91501-970, Porto Alegre, RS, Brazil
J. J. CLARIÁ[1]
Observatorio Astronómico, Universidad Nacional de Córdoba, Laprida 854, 5000 Córdoba, Argentina
AND
I. PUERARI
Instituto Nacional de Astrofisica, Optica y Electrónica, Apartado Postal 216, 72000 Puebla, Mexico
Received 1993 January 28; accepted 1995 October 13

ABSTRACT

The spatial distributions of SWB I [$10 \lesssim t$(Myr) $\lesssim 30$] and SWB II [$30 \lesssim t$(Myr) $\lesssim 70$] LMC clusters are analyzed using the enlarged sample of integrated *UBV* photometry of star clusters and associations published by Bica et al. in 1996. The differences in the clusters' spatial distributions are interpreted as dating back from their formation epoch and as being caused by a perturbation in the gaseous disk generated by the LMC stellar bar. The two SWB distributions present noncoincident bar or barlike structures with a position angle difference of $\approx 22° \pm 2°$, which, together with the age difference between the groups, leads to a perturbation propagation velocity of 13.7 ± 2 km s^{-1} kpc^{-1}, which suggests bar-induced star formation effects on the disk. Differences are also observed in the outer parts of the SWB I and SWB II spatial distributions. A spatial Fourier analysis reveals the predominance of $m = 1$ and $m = 2$ components in both cases. The spatial distribution of clusters younger than 10 Myr (SWB 0) is also studied. The patterns measured by the Fourier analysis for the SWB 0 clusters resemble the gas distribution in the potential of disk models with an off-center bar. The H I kinematics is also evidence of the presence of the perturbation in the LMC disk. Although some evidence of locally induced star formation effects is found, our analysis indicates that globally triggered star formation effects induced by the potential play an important role in organizing the overall patterns and the loci of Shapley's Constellations.

Subject headings: galaxies: kinematics and dynamics — galaxies: structure — Magellanic Clouds — open clusters and associations: general

1. INTRODUCTION

The spatial distribution of LMC clusters, divided into age groups (e.g., SWB types; Searle, Wilkinson, & Bagnuolo 1980), can be used to study the present state of different age structures. Integrated *UBV* photometry of 147 LMC star clusters allowed van den Bergh (1981) to analyze the overall spatial distribution in terms of four age groups. He concluded that very young clusters in the LMC (SWB I and younger) are concentrated in Shapley's Constellations and that the centroid of the old clusters (SWB V and older) is displaced from the centroid of the bar. Different types of objects in the LMC do not share the same centroid (de Vaucouleurs & Freeman 1973). The youngest stellar generation in the LMC, still undergoing the H II region phase, reveals large-scale structures that appear to have a counterpart in the hot dust distribution (Laspias & Meaburn 1991).

Recently, Bica et al. (1996) enlarged the *UBV* integrated photometry of star clusters and associations in the LMC to 504 and 120 objects, respectively. They measured SWB types for the whole sample using the $(U-B) \times (B-V)$ diagram. The following main conclusions were drawn about the spatial distributions of the different age groups: (1) They increase steadily with age (SWB type); (2) a difference of axial ratios exists between the groups younger and older than 30 Myr, which (assuming that the intrinsic distributions are flat and circular) implies a nearly face-on orientation for the former and a tilt $\approx 45°$ for the latter; and (3) asymmetries are present, which, together with the noncoincidence of the centroids for the different age groups, suggest that the LMC disk was severely perturbed in the past, possibly as a result of the interaction with the SMC. The number of clusters in each group is considerable, particularly for the three younger groups (138 SWB 0, 130 SWB I, and 65 SWB II objects). Tests on the statistical significance of internal structures in the spatial distributions are discussed in the present work (§ 3). The history of star formation in the LMC bar region was discussed by Bica, Clariá, & Dottori (1992, hereafter BCD92), based on part of the sample of Bica et al. (1996).

Bars are a common phenomenon in late-type spirals and Magellanic irregulars (de Vaucouleurs & Freeman 1973). An off-center bar produces perturbations on the disk, drags gas into a dominant quasi-stationary one-armed structure, and creates a second bar that is shifted with respect to the galaxy's initial stellar bar, in the direction of the disk rotation (Colin & Athanassoula 1989, hereafter CA89).

In the present paper, we interpret the internal structures in the spatial distributions of the younger groups SWB 0, SWB I, and SWB II [age ranges t(Myr) $\lesssim 10$, $10 \lesssim t$(Myr)

[1] Visiting Astronomer, Complejo Astronómico El Leoncito operated under agreement between the Consejo Nacional de Investigaciones Científicas y Técnicas de la República Argentina and the National Universities of La Plata, Córdoba and San Juan, Argentina.
[2] Visiting Astronomer, Cerro Tololo Inter-American Observatory, Chile.

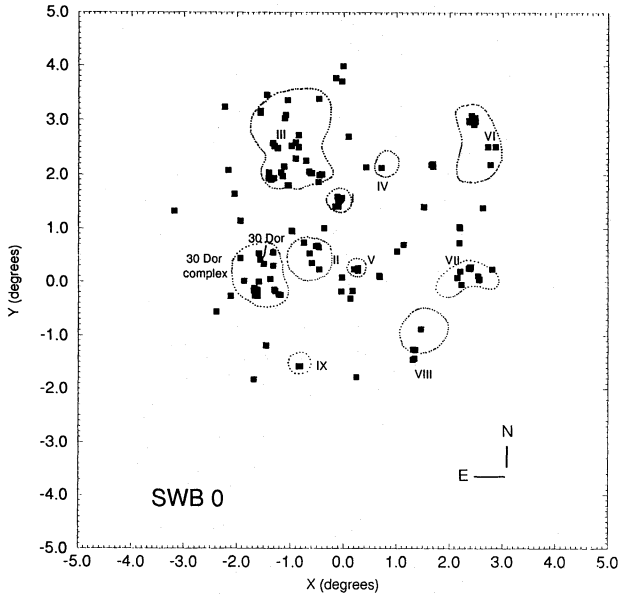

FIG. 1*a*

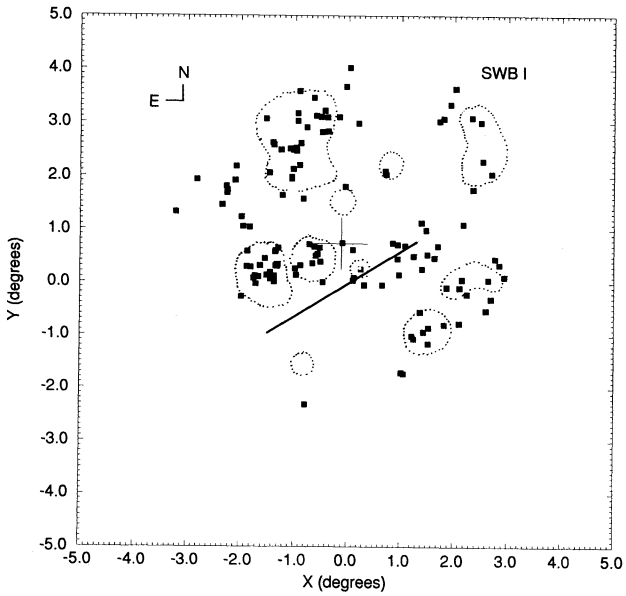

FIG. 1*b*

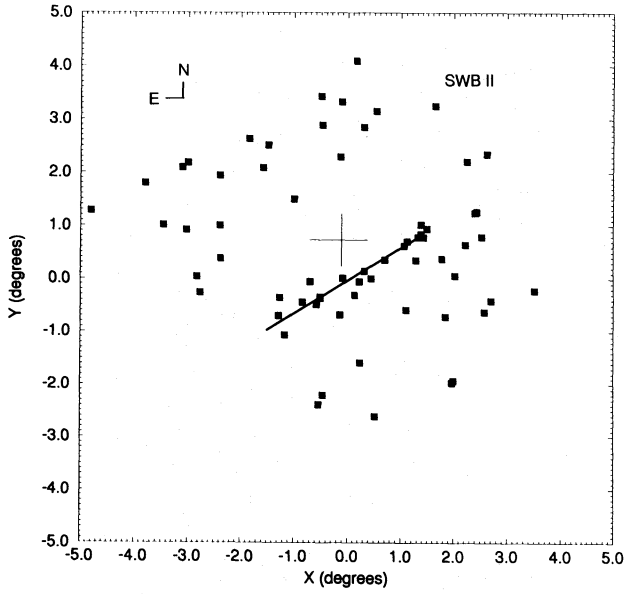

FIG. 1*c*

FIG. 1.—Spatial distribution of groups (*a*) SWB 0, (*b*) SWB I, and (*c*) SWB II. The line in (*b*) and (*c*) indicates the position and length of the stellar bar axis (de Vaucouleurs & Freeman 1973). Feast's (1964) rotation center ($J = 1950$, $\alpha = 5^h20^m$, $\delta = -68°.8$) is indicated by a cross. The loci of Shapley's Constellations and the 30 Dor complex are indicated in (*a*) and (*b*).

$\lesssim 30$, and $30 \lesssim t(\mathrm{Myr}) \lesssim 70$, respectively; see BCD92] and connect them into an evolutionary scenario caused by a disk perturbation. We infer the gravitational potential perturbations at each epoch of cluster formation and the initial dynamical evolution of such structures. The analysis is performed in two ways: (1) by deriving structural and kinematical parameters directly from the spatial distribution of data points and (2) by applying a Fourier transform method to perform a component analysis, which in turn might provide information on global star formation mechanisms.

In § 2 we analyze the structures in the spatial distribution of the young SWB groups from Bica et al. (1996). In particular, we discuss the presence of a rotated bar in the distribution of the SWB I group with respect to the LMC stellar bar and consider its kinematical implications. In § 3 we perform a structural analysis using the Fourier transform method and compare the results with those predicted by theoretical models. In § 4 we analyze the effects of the perturbation on the kinematics and distribution of H I. The conclusions of this work are given in § 5.

2. INTERNAL STRUCTURES IN THE SPATIAL DISTRIBUTIONS

The SWB 0, I, and II groups (Fig. 1) are all interior to diameters of about 6°, 6°, and 7°, respectively. These regions are considerably smaller than those occupied by intermediate-age and old clusters (Irwin 1991; Bica et al. 1996). In Figures 1*a* and 1*b* we superimpose the loci of Shapley's Constellations and the 30 Dor complex (van den Bergh 1981). The general similarities between the distribution of SWB 0 and SWB I clusters and Shapley's Constellations provides hints on how these regions have formed stars in the last 30 Myr. In these age groups a significant fraction of the objects are clumped into the Constellations, which is not the case for group SWB II (Fig. 1*c*).

The spatial distributions of the groups SWB I and SWB II indicate the presence of bars, which, however, do not coincide spatially. Their position angles (using the convention N = 0°, E = 90°) are 95° ± 1° and 117° ± 1°, respectively (see also Fig. 2). Clusters and associations surrounding the bar in each group are not uniformly distributed, with few objects in the northwest and southeast quadrants. In addition, the northeast quadrant is more populated than the southwest one. We also indicate in Figures 1*b* and 1*c* the axis of the LMC stellar bar according to the blue light central isophotes ($B \leq 21.70$ mag arcsec^{-2}) from Figure 10 of de Vaucouleurs & Freeman (1973). The axis of the stellar bar is almost aligned with the SWB II bar (Fig. 1*c*), while the SWB I bar is remarkably rotated (Fig. 1*b*). The extremes of the stellar bar axis correspond to the isophotal level $B = 22.05$ mag arcsec^{-2}, where we assume as the stellar bar length 3°.3 (corresponding to 3.0 kpc for the LMC distance modulus $[M-m] = 18.6$). The western

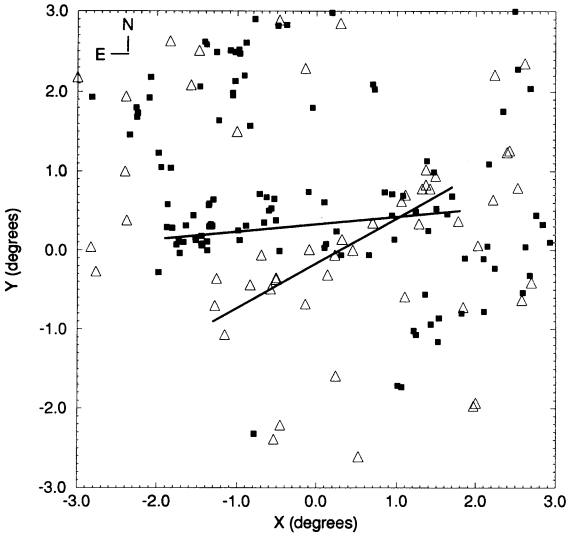

FIG. 2.—Blowup of the bar region. Lines show the position and length of the SWB I (*filled squares*) and SWB II (*open triangles*) bar axes. Notice that they cross each other on the western side and present a relative rotation.

end of the stellar bar coincides with those of the SWB I and SWB II groups within a 10% uncertainty.

2.1. *The Morphology of the SWB I and SWB II Groups*

The blowup for the bar region in Figure 2 shows the superimposition of SWB I and SWB II distributions. The lines represent the axes of their respective bars. They show a relative angular displacement of $22° \pm 2°$, with rotation center at ($X \approx 1.^{\circ}30$, $Y \approx 0.^{\circ}45$). A possible interpretation for this clockwise rotation of the SWB I bar with respect to that of the SWB II group is a perturbation propagating in the disk, which induced star formation.

The angular velocity of the perturbation, Ω_p, can be estimated from the bar angular shift ($22° \pm 2°$) and the age difference ($\Delta t \approx 30$ Myr) between the SWB I and SWB II groups, together with the distance from the eastern tip of the bars to the rotation center ($\approx 3.^{\circ}08$ or 2.83 kpc). We derive $\Omega_p = 13.7 \pm 2$ km s^{-1} kpc^{-1}. The sound velocity in the interstellar medium is typically 2–10 km s^{-1} for the wide temperature range of 300–5000 K (Allen 1973, p. 97). Consequently, supersonic velocities would be present in the eastern half of the young bar, attaining $v \approx 40$ km s^{-1} at the eastern tip. Such high shock velocities might be responsible for the formation of the 30 Dor H II complex (see Fig. 1*a*).

According to CA89, the gas response to the potential produced by the combination of a disk and off-center bar leads to gas accumulation in a one-armed structure, plus a bar that is displaced with respect to the old stellar bar of the galaxy in the same direction of the disk rotation. The LMC disk rotates clockwise, since the eastern side of the LMC disk is the nearest one to the Sun (Westerlund 1990) and the northern side of the line of nodes is receding (Feast 1964; Luks & Rohlfs 1992). The relative position of the SWB I and SWB II bars and the LMC clockwise disk rotation indicate that the bar perturbation is trailing, in agreement with the models of CA89.

It is noteworthy from Figure 2 that the SWB I and the SWB II bar axes cross each other close to their western ends. This indicates that the bar-induced perturbation is not symmetric with respect to the bar center. This effect also occurs for large longitudinal and transversal bar displacements in CA89 (e.g., their models D5 A90 and D5 A0, respectively). The stellar bar in the LMC appears to present both types of displacement, since the line joining its center to that of the disk (as defined by Feast 1964, using the rotation curve derived from the H II regions) is not perpendicular to the bar axis (Figs. 1*b* and 1*c*). As a consequence, the symmetry of the potential with respect to that line, which was assumed in CA89's models, does not occur in the LMC. The present position of the stellar bar might be indicating that it does not spin around its center with the same angular velocity as it turns around the disk center. So far, theoretical models assume the latter condition (e.g., de Vaucouleurs & Freeman 1973; CA89; Athanassoula 1992).

3. FOURIER ANALYSIS

Different authors argued for spiral patterns in the LMC disk (de Vaucouleurs & Freeman 1973; Schmidt-Kaler 1977). Usually the spiral arms have been fitted by hand, a procedure that is not objective enough for using the results to derive physical parameters. Kalnajs (1975) proposed a method based on spatial Fourier analysis to give an objective description of spiral arms.

To study in more detail the overall structure of the age groups and to give a mathematical description in terms of main pattern components, we now present an application of a spatial Fourier transform analysis to the data points in the age groups SWB 0, SWB I, and SWB II. The method, as described and applied to spiral galaxies (including some barred ones) by Puerari & Dottori (1992), is based on a Fourier decomposition of a given distribution of coplanar points into a superimposition of m-armed logarithmic spirals, having the pitch angle (i) and the number of arms (m) as parameters. Several authors agree that logarithmic spirals are the best functions to describe spiral galaxies (Boeshaar & Hodge 1977; Grosbøl 1980). Kennicutt (1981) concluded that logarithmic and hyperbolic functions fit the observed patterns in spiral galaxies well.

Mathematically, logarithmic spirals are described by

$$r = r_0 e^{(-m/p)\theta} .$$

For a distribution of points (θ, log r), the Fourier transform amplitude is given by

$$A(p, m) = \sum_{j=1}^{N} e^{-i(p \log r_j + m\theta_j)} ,$$

where p is related to the pitch angle by $\tan i = -m/p$. The results provide the relative amplitude, $A(p, m)$. We consider a peak in $A(p, m)$ to be significant if $A(p, m) \geq 4\ \sigma$, where $\sigma = N^{-1/2}$ is the Poissonian noise given by the number of clusters N. We adopted 4 σ because a series of 20 tests with randomly distributed points, with N equal to those in our groups, provided in all cases $A(p, m) \leq 2\ \sigma$. The 4 σ criterion ensures that we are dealing with significant internal structures in the spatial distributions. The more probable $A(p, m)$ values are selected by the program, and the theoretical spatial distributions of these components are retrieved by means of the inverse Fourier transform. The superposition of the main components creates the Fourier image.

In Table 1 we give for the SWB 0, SWB I, and SWB II groups the relevant m components, their respective pitch angle, and the signal-to-noise ratio (S/N) of the $A(p, m)$ peak.

TABLE 1

FOURIER ANALYSIS MAIN COMPONENTS

Group[a]	m[b]	i[c]	S/N[d]
SWB 0	1	−26°.5	4.5
	3	31.0	4.0
SWB I.....	1	−45.0	5.7
	2	−34.0	6.0
SWB II.....	1	26.0	5.1
	2	−45.0	4.0

[a] Age groups.
[b] Number of arms for the dominant logarithmic spirals.
[c] Pitch angle, where negative and positive values indicate, respectively, leading and trailing arms.
[d] Signal-to-noise ratio of the Fourier transform amplitude peak.

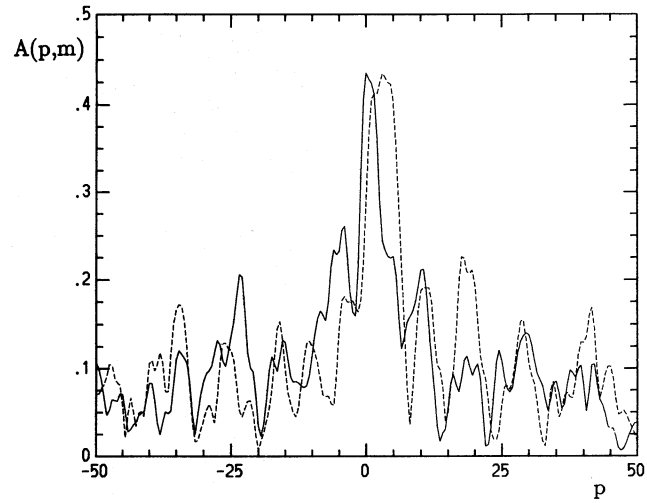

FIG. 3.—Fourier transform $A(p, m)$ for the SWB I group. The variable p is related to the pitch angle i by $\tan i = -m/p$. Only the significant components, $m = 1$ (*solid line*) and $m = 2$ (*dashed line*), are shown. Notice that the maxima do not coincide.

3.1. *Results for the SWB I and SWB II Groups*

We illustrate in Figure 3 a spatial Fourier transform histogram $A(p, m)$. It shows for the SWB I group the relevant components, $m = 1$ and $m = 2$. The remaining components are at the noise level, and, consequently, they were discarded in the construction of the Fourier image (Fig. 4). Figure 5 shows the Fourier image of the SWB II group, in which $m = 1$ and $m = 2$ are the relevant components (Table 1). The bars are mainly described by the inner part of the $m = 2$ components. The external structure is dominantly described by a radially extended $m = 1$ component, which is complemented by that with $m = 2$. The bar angular shift effect between SWB I and SWB II (§ 2.1) also shows up clearly in a comparison of the Fourier images (Figs. 4 and 5). The asymmetries in the cluster spatial distribution discussed in § 2 (Figs. 1*b* and 1*c*) are also reproduced in the Fourier images.

Taking into account the disk rotation direction discussed in § 2.1, the sum of $m = 1$ and $m = 2$ components for SWB I

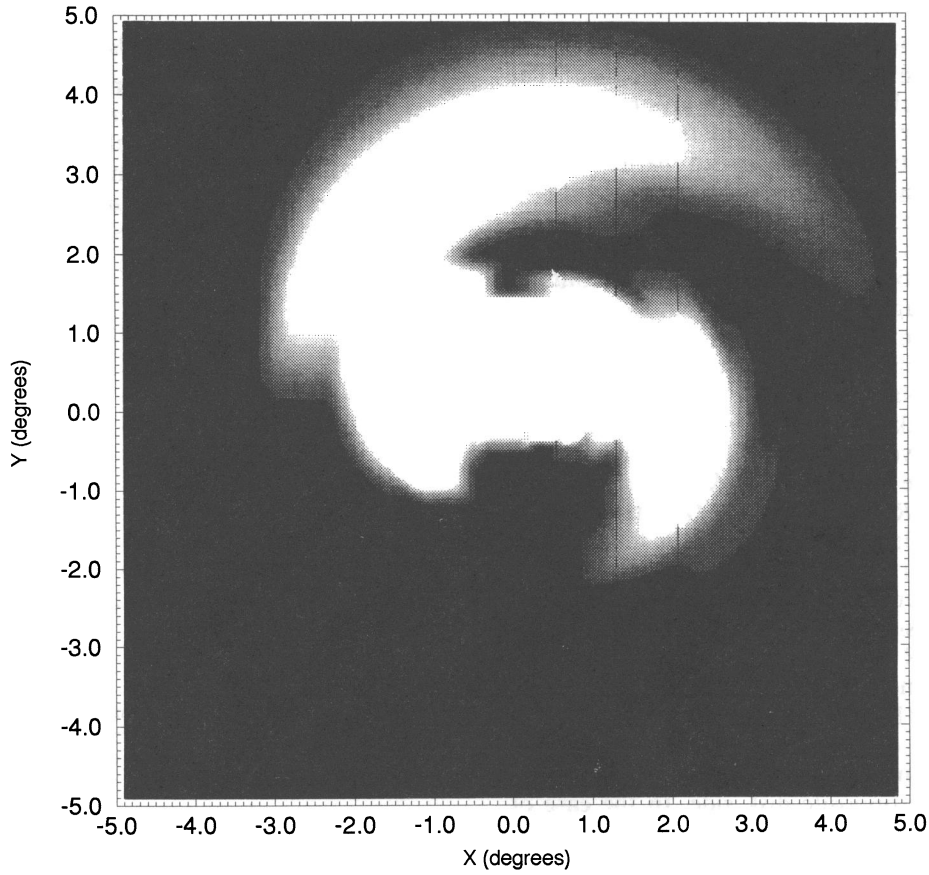

FIG. 4.—Spatial restitution (antitransform) of the Fourier transform main components for the SWB I group (those in Fig. 3). The bar and the one-armed structure are clearly seen.

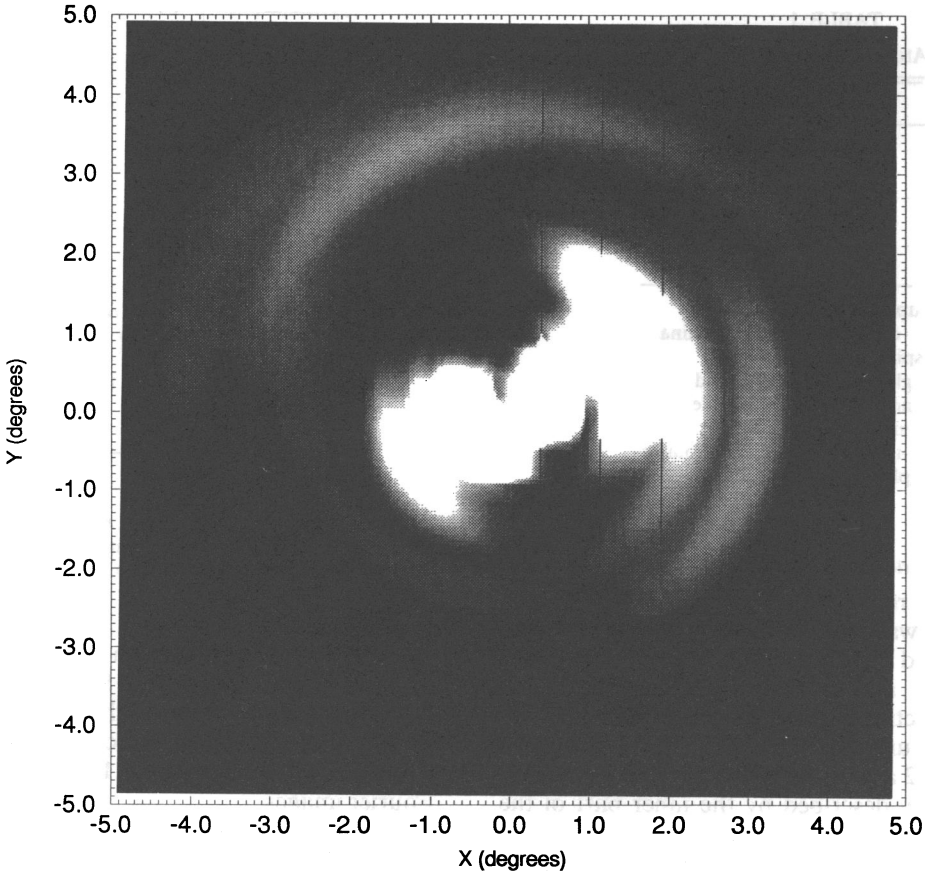

FIG. 5.—Same as Fig. 4, but for group SWB II

and SWB II produces a leading winding pattern, even when the SWB II group presents a trailing $m = 2$ component. The resulting leading wave character for both groups does not coincide with CA89's models, where all the cases of off-center bars produced trailing one-armed patterns. Two interpretations are possible for this effect. The first one is that at the formation epoch the patterns were indeed trailing, as in CA89's models (see also our discussion in § 3.2 for the SWB 0 group), but because of the dynamical evolution of the newborn stellar aggregates throughout the disk, the structure could be deformed into one with a leading appearance. The second interpretation relies on the possibility of absence of inner Lindblad resonances (ILRs), so that the perturbation can overtake the disk center emerging on the opposite side with a reversed wave character. In order to check this possibility we follow Binney & Tremaine (1987, p. 349). We derived $\Omega(R) \pm (\kappa/2)$ (where Ω is the angular velocity, κ is the epicycle frequency, and R is the distance from the rotation center) for the LMC (Fig. 6), using Feast's (1964) LMC rotation curve. The rotation curve of Luks & Rohlfs (1992) provides similar results. The behavior of the curve $\Omega(R) - (\kappa/2)$ as $R \rightarrow 0$ is a signature of a potential without ILRs. The absence of an ILR, as argued by Binney & Tremaine (1987, p. 381), allows a perturbation to propagate freely through the disk center and, consequently, to change its character from trailing to leading or vice versa, when it emerges on the opposite disk side. In the case of CA89's models, they use the superposition of a very concentrated and an extended Toomre disk, which causes the existence of an ILR as shown by Sanders & Tubbs (1980) for the potential adopted by CA89.

3.2. *SWB 0: The Youngest Group*

The Fourier analysis of group SWB 0 indicates that the dominant components are $m = 1$ and $m = 3$ (Table 1). In Figure 7 we show the radial density distribution of these components, which is obtained by azimuthally integrating the corresponding Fourier image. A density minimum in the radial distribution occurs for both components at about $R = 1^{\circ}.9 \pm 0^{\circ}.2$ (≈ 1.7 kpc $\pm$ 0.2 kpc). We interpret this

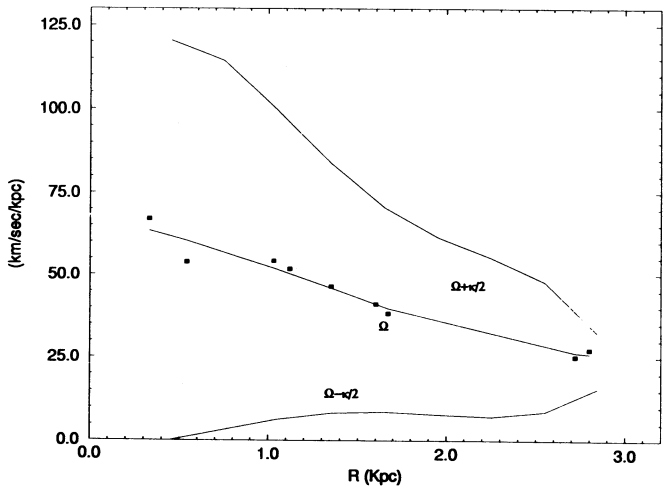

FIG. 6.—The angular velocity Ω and $\Omega \pm (\kappa/2)$ (κ is epicycle frequency) as a function of radius. We used Feast's (1964) rotation curve; the rotation curve of Rohlfs et al. (1984) provides comparable results. The behavior of $\Omega - (\kappa/2)$ implies that inner Lindblad resonances do not occur in the LMC disk (§ 2.2).

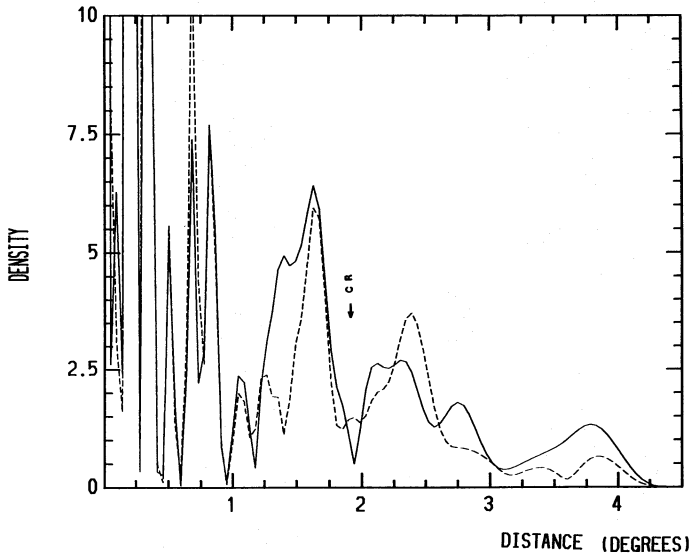

FIG. 7.—Radial density distribution of the $m = 1$ (*solid line*) and $m = 3$ (*dashed line*) components for the SWB 0 group. The low-density zone at $1^\circ.9 \pm 0^\circ.2$ is interpreted as the corotation radius (CR).

region as corresponding to the corotation circle (CR). The CR can be seen in the Fourier image as the sharp south-southeast circular edge in Figure 8*a*. To the west it marks the inner edge of Shapley VII ($X \approx 2^\circ.4$, $Y \approx 0^\circ.1$; see also Fig. 1*a*). Finally, to the northeast it traces the separation between Shapley III ($X \approx -1^\circ.0$, $Y \approx 2^\circ.6$) and the more internal complexes 30 Dor, Shapley II, and Shapley I. The eastern tip of the stellar bar, as well as those of the SWB I and SWB II groups, end at CR. On the other hand, CR occurs $\approx 20\%$ farther out from the western tips of the bars. This displacement of CR with respect to the bar end also occurred in CA89's disk plus asymmetric bar potential models.

The Fourier image of SWB 0 (Fig. 8*a*) can be compared to the response to the gas in the potential of one of the off-center bar models of CA89 (their model D5 A90). We recall that in all of their models, the one-armed structure is trailing. The one-armed pattern in our SWB 0 Fourier image is also trailing, in agreement with the models. As discussed in § 3.1, the leading character of the SWB I one-armed structure might result from a change in the perturbation character due to the absence of an ILR. The difference in the winding character between SWB 0 and SWB I suggests that such changes might occur in a timescale of 10–20 Myr.

It is worth noting that local density maxima occur in the one-armed structure of CA89's models (e.g., Fig. 8*b*), in spite of the fact that the initial gas distribution in their models is homogeneous. Concentrations also occur in the Fourier images (Fig. 8*a*), which suggest that the loci of the large Shapley's Constellations can be induced by the potential and not necessarily by initial inhomogeneities in the distribution of gas clouds and/or stochastic propagation of star formation. Nevertheless, there exists evidence of locally induced star formation processes, such as bubbles from supernova and massive star winds, in the LMC (Braunsfurt & Feitzinger 1983). There is also evidence of self-propagating star formation, as can be seen in Shapley III (Figs. 1*a* and 1*b*), since present star formation (SWB 0) is concentrated in the southern part of the Constellation.

4. IS THE PERTURBATION AFFECTING H I?

Luks & Rohlfs (1992) have kinematically decomposed the LMC H I distribution in the inner $8^\circ.4 \times 8^\circ.4$ into a flat disk with a symmetric rotation curve and a lower velocity component (therein called the L component) that contains 19% of the H I. It has two lobes (see their Fig. 15) referred to as northern and southern ones. As studied in detail for M81 by Visser (1980), in spiral galaxies a low-velocity component, coincident with the H I maxima, appears as a perturbation on the velocity field of a disk. Interpreting the LMC H I L component in a similar way, we superimposed it onto our data points for the SWB I and SWB II groups in Figure 9. A bar structure oriented in the east-west direction can be identified in the northern lobe. It is rotated clockwise by an angle of $\approx 30^\circ$ with respect to the SWB II bar, and consequently it is ahead $\approx 8^\circ$ with respect to that of SWB I (§ 2.1).

The H I barlike structure stretched in the east-west direction is interpreted as the material that is being presently accumulated by the potential, such that it should trace the present position of the perturbing pattern. The H I bar appears to share the same rotation center as that of the SWB I and SWB II bars (see also Fig. 2).

The angular velocity of the pattern derived from this angle and the bar length quoted in § 2.1 is 12.5 km s^{-1} kpc^{-1}, in good agreement with the value 13.7 km s^{-1} kpc^{-1} derived from the SWB I and SWB II groups in § 2.1. The southern lobe of the L component seems to be the more developed feature of a one-armed structure. It is trailing like the bar in the SWB 0 group distribution.

5. CONCLUDING REMARKS

The spatial distribution of the SWB 0, SWB I, and SWB II age groups were studied. The SWB I group presents a bar that is rotated with respect to that of SWB II group, which in turn coincides with the LMC stellar bar. Their relative position allows one to infer the presence of a perturbation pattern that propagates at 13.7 km s^{-1} kpc^{-1}. A bar structure can also be identified in the low-velocity component of the H I distribution, which provides a perturbation velocity of 12.5 km s^{-1} kpc^{-1}, in good agreement with that deduced from the SWB I and SWB II groups.

The Fourier analysis shows that one- and two-armed components are dominant in the SWB I and SWB II groups. On the other hand, for the SWB 0 group, one- and three-armed components prevail. The Fourier image shows that the SWB I and SWB II groups present a leading one-armed pattern outside the bar, while the SWB 0 group presents a trailing pattern in the same region. This behavior of the SWB 0 group is in agreement with the predictions of the models of CA89. The leading pattern in SWB I and SWB II groups might be due to the absence of inner Lindblad resonance in the LMC disk, as inferred from the rotation curve. This property allows a perturbation to move freely across the disk center and, consequently, to change its winding character from trailing to leading or vice versa. The line joining the disk and bar centers is not perpendicular to the stellar bar axis, which suggests that the bar might be spinning around its center with an angular velocity different from that with which it turns around the disk center. It would be important that LMC models take into account this kinematical asymmetry.

It is known that star formation induced by shells occurs in the LMC. Nevertheless, the present study shows that

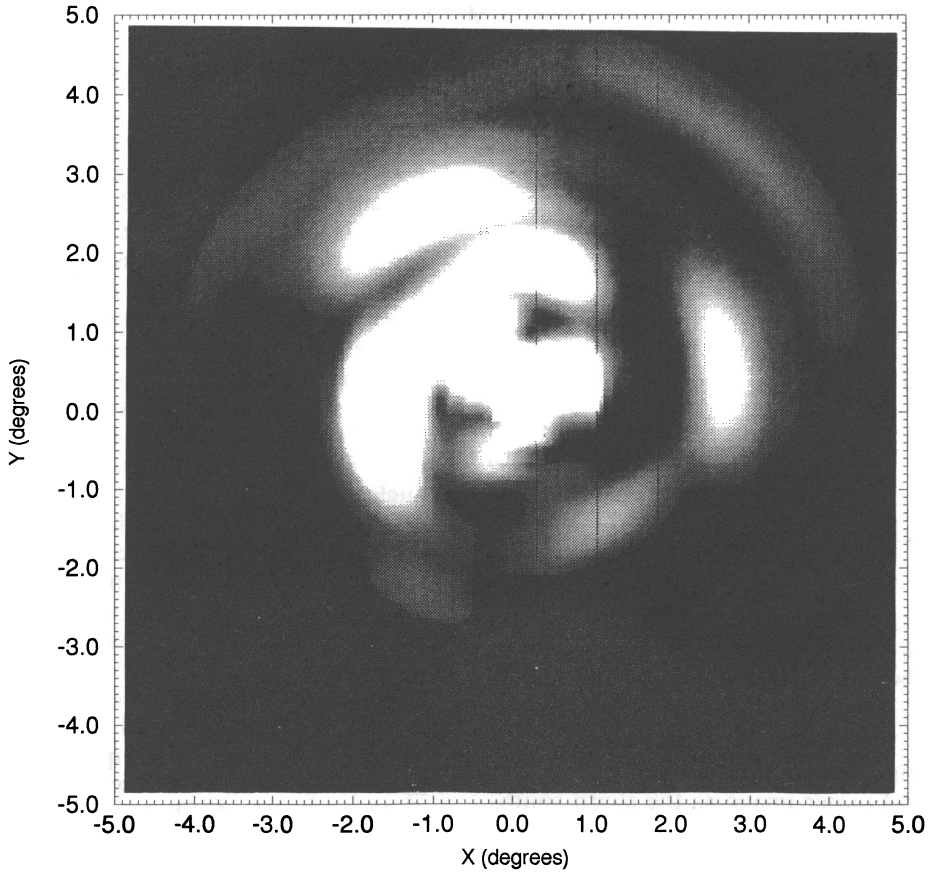

FIG. 8*a*

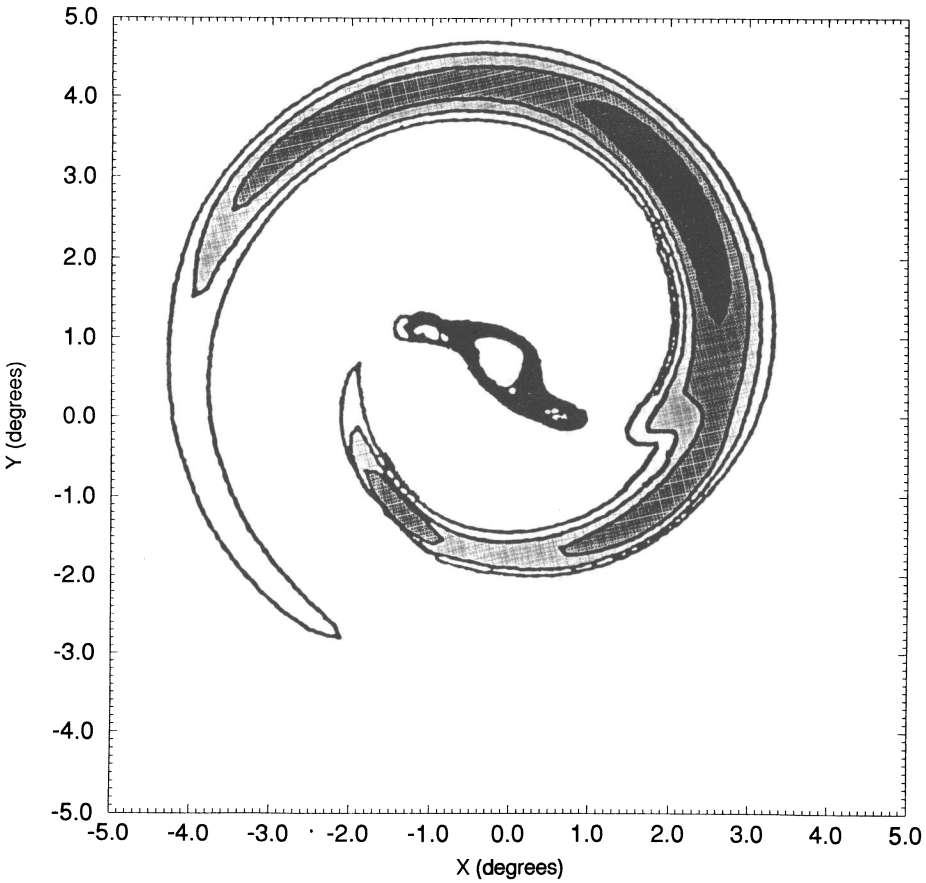

FIG. 8*b*

FIG. 8.—(*a*) Spatial restitution of the Fourier transform main components for the SWB 0 group. (*b*) CA89's model D2 A90 for an off-center bar displaced perpendicular to the bar's major axis.

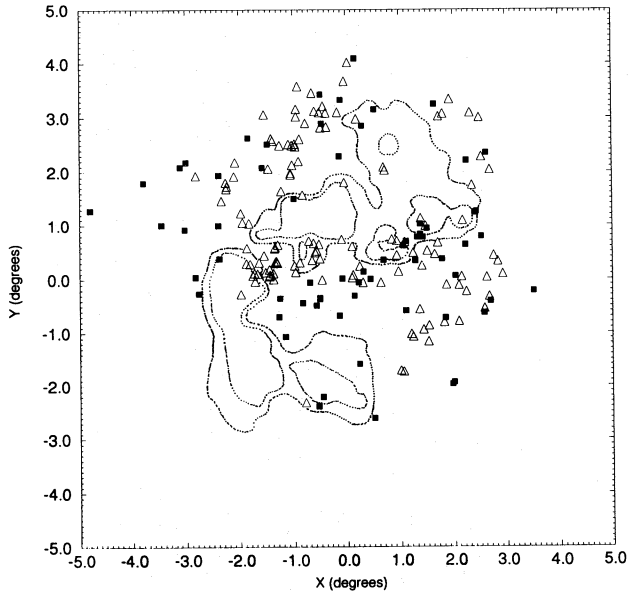

FIG. 9.—The high-velocity H I isodensities of Luks & Rohlfs (1992) (their L component) superimposed on the distribution of SWB I (*open triangles*) and SWB II (*filled squares*) groups. The L component barlike structure is displaced to the north and rotated 30° clockwise with respect to that of the SWB II group. The disk rotation center position (cross in Figs. 1*b* and 1*c*) of Feast (1964) suggests the bar perturbation overtook it and is presently located on the opposite side of the disk.

global processes associated with the bar plus disk potential play a fundamental organizing role in triggering star formation. These properties remain frozen in the spatial distribution of the young stellar population for up to ≈ 50 Myr.

We thank the staffs at CTIO and CASLEO for the hospitality and assistance during the observing runs. I. P. acknowledges a CNPq fellowship during a period of his Ph.D. in France. We are grateful to Alessandro Bachieri and Fábio Perosi for the help in the computations, tables, and figures. We also thank an anonymous referee for interesting remarks. This work was partially supported by the Brazilian institutions CNPq and FAPERGS, as well as by CONYCET and CONICOR from Argentina.

REFERENCES

Allen, C. W. 1973, Astrophysical Quantities (3d ed.; London: Athlone)
Athanassoula, E. 1992, MNRAS, 259, 328
Bica, E., Clariá, J. J., & Dottori, H. 1992, AJ, 103, 1859 (BCD92)
Bica, E., Clariá, J. J., Dottori, H., Santos, J. F. C., Jr., & Piatti, A. 1996, ApJS, 102, 57
Binney, J., & Tremaine, S. 1987, Galactic Dynamics (Princeton: Princeton Univ. Press)
Boeshaar, G. O., & Hodge, P. W. 1977, ApJ, 213, 361
Braunsfurth, E., & Feitzinger, J. V. 1983, A&A, 127, 113
Colin, J., & Athanassoula, E. 1989, A&A, 214, 99 (CA89)
de Vaucouleurs, G., & Freeman, K. C. 1973, Vistas Astron., 14, 163
Feast, M. V. 1964, MNRAS, 127, 195
Grosbøl, P. J. 1980, in ESO Workshop on Two Dimensional Photometry, ed. P. C. Crane & K. Kjär (Garching: ESO), 261
Irwin, M. J. 1991, in IAU Symp. 148, The Magellanic Clouds, ed. R. Haynes & D. Milne (Dordrecht: Kluwer), 453
Kalnajs, A. J. 1975, in La Dynamique des Galaxies Spirales, Colloq. Internat. CNRS 241, ed. L. Weliachew (Paris: Editions CNRS), 103
Kennicutt, R. C., Jr. 1981, AJ, 86, 1847
Laspias, V. N., & Meaburn, J. 1991, MNRAS, 249, 1P
Luks, Th., & Rohlfs, K. 1992, A&A, 263, 41
Puerari, I., & Dottori, H. 1992, A&A, 93, 469
Rohlfs, K., Kreitchmann, J., Siegman, B. C., & Feitzinger, J. V. 1984, A&A, 137, 343
Sanders, R. H., & Tubbs, A. D. 1980, ApJ, 235, 803
Schmidt-Kaler, Th. 1977, A&A, 54, 771
Searle, L., Wilkinson, A., & Bagnuolo, W. G. 1980, ApJ, 239, 803
van den Bergh, S. 1981, A&AS, 46, 49
Visser, C. D. 1980, A&A, 88, 159
Westerlund, B. E. 1990, A&ARev., 2, 29